Dynamic Effects of Linkage Joints in Electrostatic Microengines

J. J. Allen, S. L. Miller, G. F. LaVigne, M. S. Rodgers
Intelligent Micro-machine Technology Department
http://www.mdl.sandia.gov/Micromachine

W. P. Eaton
Reliability Physics Department
Sandia National Laboratories
Albuquerque, NM, 87185

Abstract

The electrostatic microengine is one of the major actuators used in MEMS applications. To ensure this MEMS actuator is operated in a fashion that will produce peak performance and long life, the system dynamics must be fully understood. One of the major trade-offs in the microengine design is the use of either pin or flexure joints. This paper will develop the equations of motion for flexure-jointed and pin-jointed surface micromachined microengines. An analytical mechanics approach will be used to derive the equations of motion and the appropriate equations of constraint. The effect of the flexure joints on the drive signals of the micro engine is experimentally shown to be significant during static tests.

Introduction

The development of actuation devices for micro-electro-mechanical systems (MEMS) is an essential advance in the development of useful MEMS devices. Sandia National Laboratories has developed the Sandia microengine [1], which has been used as actuation for a number of applications [2,3], such as optical shutters, gear reduction units, linear racks, and a counter-meshing gear discriminator [4]. The microengine shown in Figure 1 consists of a pinion gear connected by linkages to two electrostatic comb drives, which supply linear forces. The development of reliable, long-life MEMS devices requires the proper understanding of the dynamics of the microengine. Previous work has been done to determine the optimum drive signals for the pin-jointed microengine [5], which has resulted in extending the operational life of the Sandia microengine over a broad range of speeds.

A significant design choice in the microengine is the use of pin-joints versus flexure joints, Figure 2, in the linkages of the microengine. The use of a pin-jointed linkages allow linkage movement which is impeded only by the friction in the pin-joint; however, the pin-joint clearances which arise from the surface micromachine fabrication technology may give rise to undesirable dynamic effects or positional inaccuracy. The use of flexure joints in the linkages removes concerns regarding the joint clearances; however, non-negligible force is required to overcome the joint stiffness during microengine operation. In order to properly operate the microengine for maximum load and system lifetime, the dynamics and design tradeoffs of the Sandia microengine must be fully understood.

This paper examines the effect of the linkage joint on microengine dynamics. Sandia microengines have been designed and fabricated with both pin joint and flexure-joint linkages shown in figure 2. This paper will derive the equations of motion for both types of microengines and the optimal drive signals required to minimize friction effects in these devices. Experimental evaluation of the effects of linkage joint type on system operation and the required drive signals will be presented.

Microengine Model

The equations of motion for the microengine will be developed using an analytical mechanics approach. The equations of motion for the pin-joint microengine have been previously developed [5] using Newton's laws. However, when complications of additional constraints or degrees of freedom, such as flexures, are added to the problem this approach becomes unwieldy. Lagrange's equations that incorporate system constraints via Lagrange multipliers will be used [6]. This approach results in $n+m$ equations for a system with $n-m$ degrees of freedom. The system

of equations which describe the system dynamics consist of n equations of motion for the n generalized coordinates of the system, and m constraint equations which relate the constrained generalized coordinates, equations 1. Upon solution of the system equations, the Lagrange multiplier, λ_i, correspond to the force required to enforce the ith constraint.

$$\frac{d}{dt}\left(\frac{\partial T}{\partial \dot{q}_k}\right)-\frac{\partial T}{\partial q_k}+\frac{\partial D}{\partial \dot{q}_k}+\frac{\partial V}{\partial q_k}=Q_k+\sum_{i=1}^{m}\left(\lambda_i\frac{g_i}{q_k}\right)$$
$$k=1\cdots n$$

(1)

$$g_i=0 \qquad i=1\cdots m$$

Figure 3 is a schematic of the microengine that show the variables, which will be used in the development of the equations of motion. The schematic will be used for both flexured and pin-joint micro engine analysis. The flexured micro engine analysis will involve torsional springs k_2, k_3, k_4 located at joints 2, 3 and 4.

Flexured Microengine

The flexured microengine equations of motion will be derived using $n=6$ generalized coordinates. The generalized coordinates, q_i, are:

- y_3, x_4 which describe the comb drive mass positions
- β_x, β_y which describe the linkage configuration
- r, θ which describe the pinion position

Since the microengine has only one independent degree of freedom which could be taken as θ, there must be $m=5$ constraint equations. The constraint equations, equation 2, for the flexured microengine relate the comb drive positions and linkage configuration which can be derived from geometric considerations. The last constraint equation, g_5, state that the linkage-pinion connection is at a constant radius, r_0.

$$g_1=y_3-L(\cos\beta_x-1)-r_0+r\cos\theta$$

$$g_2=x_4-\frac{L_1 r\sin\theta}{L}+L_3(1-\cos\beta_y)$$

$$g_3=\sin\beta_x-\frac{r\sin\theta}{L}$$

(2)

$$g_4=\sin\beta_y-\frac{L_2(\cos\beta_x-1)}{L_3}+\frac{r\cos\theta}{L_3}-\frac{r_0}{L_3}$$

$$g_5=r-r_0$$

The kinetic, potential and dissipation functionals (T, V, D respectively) can be written

as shown in equations 3. Equations 3 also show the generalized forces, Q_i, for the system.

$$T=\frac{1}{2}m_y\dot{y}_3^2+\frac{1}{2}m_x\dot{x}_4^2$$

$$V=\frac{1}{2}k_x x_4^2+\frac{1}{2}k_y y_3^2+\frac{1}{2}k_2(\beta_x+\beta_y)^2$$
$$+\frac{1}{2}k_3\beta_x^2+\frac{1}{2}k_4\beta_y^2$$

(3)

$$D=\frac{1}{2}c_x\dot{x}_4^2+\frac{1}{2}c_y\dot{y}_3^2$$

$$Q_1=F_y \quad Q_2=F_x \quad Q_3=0 \quad Q_4=0$$

$$Q_5=0 \quad Q_6=F_l r$$

The application of Lagrange's equations, equations 1, yield equations 4, which along with the constraints, equations 2 fully describe the flexured microengine system dynamics. The radial force at the pinion, F_r, has been substituted for the Lagrange multiplier, λ_5, because this is the force required to enforce constraint g_5.

$$m_y\ddot{y}_3+c_y\dot{y}_3+k_y y_3-F_y-\lambda_1=0$$

$$m_x\ddot{x}_4+c_x\dot{x}_4+k_x x_4-F_x-\lambda_2=0$$

$$k_3\beta_x+k_2(\beta_x+\beta_y)-\lambda_1 L\beta_x-\lambda_3$$
$$-\frac{\lambda_4 L_2\beta_x}{L_3}=0$$

$$k_4\beta_y+k_2(\beta_x+\beta_y)-\lambda_2 L_3\beta_y-\lambda_4=0$$

(4)

$$-\lambda_1\cos\theta+\frac{\lambda_2 L_1\sin\theta}{L}+\frac{\lambda_3\sin\theta}{L}$$
$$-\frac{\lambda_4\cos\theta}{L_3}-F_r=0$$

$$-F_l r+\lambda_1 r\sin\theta+\frac{\lambda_2 L_1 r\cos\theta}{L}+\frac{\lambda_3 r\cos\theta}{L}$$
$$-\frac{\lambda_4 r\sin\theta}{L_3}=0$$

Pin-jointed Microengine

Since there is no flexure potential energy to be described mathematically, the pin-jointed microengine can be modeled using 4 generalized coordinates which describe the comb drive mass positions (x_4, y_3) and pinion position (r, θ). Once again the microengine has 1 independent degree of freedom, and the 3 relevant system constraints, equations 5, relate the comb drive position and pinion position. Also the pinion linkage connection is once again at a constant radius, r_0. The pin-joint microengine constraints are a subset of the flexure-jointed microengine constraints.

$$g_1 = y_3 - r_0 + r\cos\theta$$

$$g_2 = x_4 - \frac{L_1 r \sin\theta}{L} \tag{5}$$

$$g_3 = r - r_0$$

Application of Lagrange's equations yield equations 6, which are a simplified subset of the flexure-joint microengine equations. The radial force at the pinion, F_r, has been substituted for the Lagrange multiplier, λ_3.

$$m_y \ddot{y}_3 + c_y \dot{y}_3 + k_y y_3 - F_y - \lambda_1 = 0$$

$$m_x \ddot{x}_4 + c_x \dot{x}_4 + k_x x_4 - F_x - \lambda_2 = 0$$

$$-\lambda_1 \cos\theta + \frac{\lambda_2 L_1 \sin\theta}{L} - F_r = 0 \tag{6}$$

$$-F_l r + \lambda_1 r \sin\theta + \frac{\lambda_2 L_1 r \cos\theta}{L} = 0$$

Comb Drive Signals

In order to minimize the friction force in the pinion hub, the optimal drive signal would produce no radial hub force, F_r. The system of equations can be rearranged to explicitly show the functional dependence of comb-drive voltages (V_x, V_y) on the system parameters. Equations in this form help to solve for the comb-drive signals required to minimize the hub radial force, F_r. The system of equations for the pin-joint and flex-joint microengines can be simplified by the following assumptions to yield equations 7 and 8. The simplifications used are:

- Assume small angle rotations for β_x and β_y since L and L_3 are long compared to the comb drive displacements. Also, products of angles β_x and β_y are negligible.
- F_x and F_y are the comb-drive electrostatic forces, which can be modeled as $a_x V_x^2$ and $a_y V_y^2$ respectively [5].
- Assume the comb-drive mass, damping, stiffness and electrostatic parameters are equal (i.e. $m_x = m_y = m$, $c_x = c_y = c$, $k_x = k_y = k$, $a_x = a_y = a$).
- ω_0 and δ are the natural frequency and damping ratio of the comb-drives.
- The flexure stiffnesses are assumed to be equal. ($k_{flex} = k_2 = k_3 = k_4$).

The flexure-jointed equations are very similar in form to the pin-jointed equations except for the additional term at the end.

Pin-Jointed Microengine:

$$V_x^2 = \frac{1}{\gamma}\frac{kr}{a}\left\{ \begin{array}{l} \frac{\gamma^2}{\omega_0^2}\left[(\ddot{\theta}+2\delta\dot{\theta})\cos(\theta)-\dot{\theta}^2\sin\theta\right] \\ +\left(\frac{F_r}{kr}+\gamma^2\right)\sin\theta + \frac{F_l}{kr}\cos\theta \end{array} \right\}$$

$$\tag{7}$$

$$V_y^2 = \frac{kr}{a}\left\{ \begin{array}{l} \frac{1}{\omega_0^2}\left[(\ddot{\theta}+2\delta\dot{\theta})\sin(\theta)-\dot{\theta}^2\cos\theta\right] \\ +\left(\frac{F_r}{kr}+1\right)\cos\theta + \frac{F_l}{kr}\sin\theta \end{array} \right\}$$

Flexure-Jointed Microengine:

$$V_x^2 = \frac{1}{\gamma}\frac{kr}{a}\left\{ \begin{array}{l} \frac{\gamma^2}{\omega_0^2}\left[(\ddot{\theta}+2\delta\dot{\theta})\cos(\theta)-\dot{\theta}^2\sin\theta\right] \\ +\left(\frac{F_r}{kr}+\gamma^2\right)\sin\theta + \frac{F_l}{kr}\cos\theta + \frac{\gamma\lambda_{2\,mod}}{kr} \end{array} \right\}$$

$$\tag{8}$$

$$V_y^2 = \frac{kr}{a}\left\{ \begin{array}{l} \frac{1}{\omega_0^2}\left[(\ddot{\theta}+2\delta\dot{\theta})\sin(\theta)-\dot{\theta}^2\cos\theta\right] \\ +\left(\frac{F_r}{kr}+1\right)\cos\theta + \frac{F_l}{kr}\sin\theta + \frac{\lambda_{1\,mod}}{kr} \end{array} \right\}$$

where,

$$\frac{\gamma\lambda_{2\,mod}}{kr} = \frac{\gamma}{L_1 L_3}\left[\begin{array}{l} LL_3\beta_x(F_l\sin\theta - F_r\cos\theta) \\ +LL_3(F_r\sin\theta + F_l\cos\theta) \\ +L_3\frac{k_{flex}}{kr}(2\beta_x + \beta_y) \end{array} \right]$$

$$\frac{\lambda_{1\,mod}}{kr} = \frac{1}{L_1 L_3}\left[\begin{array}{l} LL_3\beta_y[F_l\cos\theta + F_r\sin\theta] \\ +L_1\frac{k_{flex}}{kr}(2\beta_y + \beta_x) \end{array} \right]$$

Experimental Verification of Microengine Equations

The pin-jointed microengine equations have been used to develop drive signals for the Sandia microengine. These drive signals have been used to drive both pin-jointed and flexure-jointed microengines. If the flexure effects on the microengine dynamics were either small or could be modeled as a simple increase in an *effective* stiffness term, the microengine drive signals would be simple to implement. It should be noted that the strain energy of the comb drive springs have maxima or minima at 0°, 90°, 180°,

270°, Figure 4. However, the flexure strain energy of joint 2 has a maxima at an angle between 90°, 180°, Figure 4, which is determined by the linkage lengths. This effect produces a phase shift in the drive signals.

An experimental comparison of the two methods for drive signal calculation can be performed using a *gearless* microengine as the characterization vehicle. The gearless microengine is a microengine with orthogonal comb drives and linkage arms, but no pinion or hub. The linkage arms for this engine are not physically constrained to circular motion. Therefore the ability of a particular set of drive signals to make the gearless microengine track a circle is a measure of the physical significance of the flexure stiffness in the micro engine.

The determination of the physical constants used in the drive signal calculations can be difficult, however, many grouped or lumped parameters can be determined. For example, the force balance of a comb drive between the restoring force of the springs and the applied electrostatic force is

$$aV^2 = kx \qquad (9)$$

where x is the linear displacement of the shuttle. In this instance, voltage can be applied and x can be measured, but only the lumped term k/a can be determined. For the drive signal equations, however, these lumped terms are sufficient for drive signal calculation. For the microengine, the important lumped parameters are kr/a and k_{flex}/kr, which can be experimentally determined by applying DC voltages to the comb drives such that the linkage arms sweep out a circle of the prescribed diameter. This data can then be used to determine the parameters kr/a and k_{flex}/kr in the pin-jointed and flex-jointed microengine equations. Since this is a DC experiment the dynamic terms ($\dot{\theta}$ and $\ddot{\theta}$) of the equations are neglected. The terms F_l and F_r are also removed, since this is a gearless microengine. The static pin-jointed equations for a gearless microengine are:

$$V_x^2 = \frac{kr}{a}\gamma\sin\theta$$

$$\qquad (10)$$

$$V_y^2 = \frac{kr}{a}(1-\cos\theta)$$

Similarly, the static flexure-jointed equations for a gearless microengine are:

$$V_x^2 = \frac{kr}{a}\left\{\gamma\sin\theta + \frac{\lambda_{2mod}}{kr}\right\}$$

$$\frac{\lambda_{2mod}}{kr} = \frac{k_{flex}}{kr}\frac{(2\beta_x + \beta_y)}{L_1}$$

$$\qquad (11)$$

$$V_y^2 = \frac{kr}{a}\left\{1-\cos\theta + \frac{\lambda_{1mod}}{kr}\right\}$$

$$\frac{\lambda_{1mod}}{kr} = \frac{k_{flex}}{kr}\frac{(\beta_x + 2\beta_y)}{L_3}$$

Figure 5 shows the results of the experimental determinations of normalized spring constants using both sets of equations. At discrete 'gear' angles, the required voltages V_x and V_y were recorded. As the graph shows, both sets of equations adequately model the motion of the y comb drive, whereas the flex joint equations are better at describing the motion of the x drive than the pin-jointed equations. The flexure-joint equations are able to adequately model the phase shift required in the x drive signal, which arises from the stiffness of the center link flexure. Figure 6 shows the significance of the correction terms λ_{1mod}/a, λ_{2mod}/a.

Summary

This paper presents a procedure for development of the pin-joint and flexure-joint microengine equations of motion. Experimental data was presented which illustrates the ability of the flexure-jointed microengine equations to model the phase shift due to the flexure-joint used in the microengine linkages. The experimental data shows the phase shift effects.

Additional work needs to be done to study the dynamics of the pin-jointed and flexure-jointed microengines over a range of operational speeds. At speeds above the natural frequency of the comb drive the inertial forces will tend to play a larger role in system dynamics. However, for low speed and positional accuracy the effects of the flexure-jointed terms have proved significant.

References

1. E. J. Garcia and J. J. Sniegowski, "Surface micromachined microengine", Sensors and Actuators A, Vol. 48, (1995) pp. 203-214.

2. J. J. Sniegowski, S. L. Miller, G. LaVigne, M. S. Rodgers, and P. J. McWhorter, "Monolithic Geared-Mechanisms Driven by a Polysilicon Surface-Micromachined On-chip Electrostatic Engine", Technical Digest of the 1996 Solid State Sensor and Actuator Workshop, Hilton Head Island, SC, June 3-6, 1996, pp. 178-182.

3. J. J. Sniegowski and E. J. Garcia, "Microfabricated actuators and their application to optics", Proc. SPIE Miniaturized Systems with Micro-Optics and Micromechanics, Vol. 2383. San Jose, CA, Feb. 7-9, 1995, pp. 46-64.

4. M. A. Polosky, E. J. Garcia, J. J. Allen, "Surface micromachined counter-meshing gears discrimination device", Proc. SPIE Smart Electronics and MEMS, San Diego, March, 1998.

5. S. L. Miller, J. J. Sniegowski, G. LaVigne, and P. J. McWhorter, "Friction in Surface Micromachined Microengines", Proc. SPIE Smart Electronics and MEMS Vol. 2722, San Diego, Feb. 28-29, 1996, p. 197-204.

6. L. Meirovitch, Methods of Analytical Dynamics, McGraw-Hill Book Company, 1970.

Nomenclature

a_x, a_y, a – comb drive electrostatic coefficients

c_x, c_y, c – comb drive damping coefficients

F_x, F_y – Forces on comb drive masses

F_l, F_r – Lateral and radial pinion gear forces

g_i, - Constraint equation

k_x, k_y, k – comb drive spring stiffnesses

k_2, k_3, k_4, k_{flex} – flexure stiffnesses

L, L_1, L_2, L_3 – Linkage lengths

m_x, m_y, m – comb drive masses

q_i, Q_i - Generalized coordinates and forces

r_0 – Pinion gear radius

T, D, V – Kinetic, Dissipation, Potential Energy functionals

x_4 – X comb drive displacement

y_3 – Y comb drive displacement

β_x, β_y – Linkage rotation angles

γ - L_1/L

λ_i – Lagrange multipliers

λ_{1mod}, λ_{2mod} – Flexure joint correction terms

θ - Pinion rotation angle

Flexure-Joints

Figure 1. Flexure-Jointed Microengine
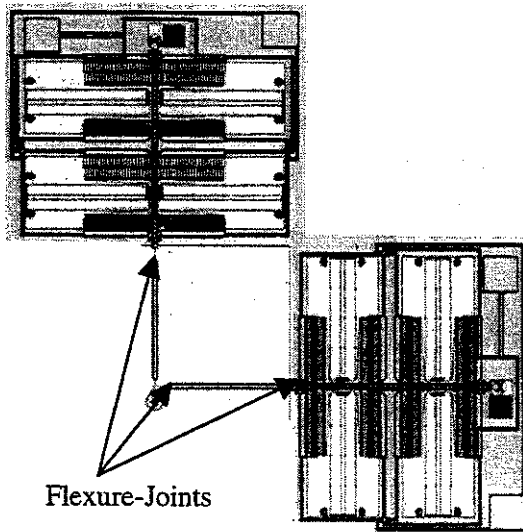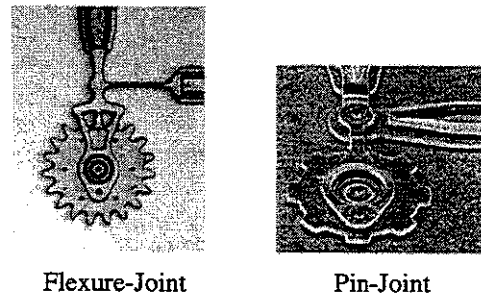

Flexure-Joint   Pin-Joint
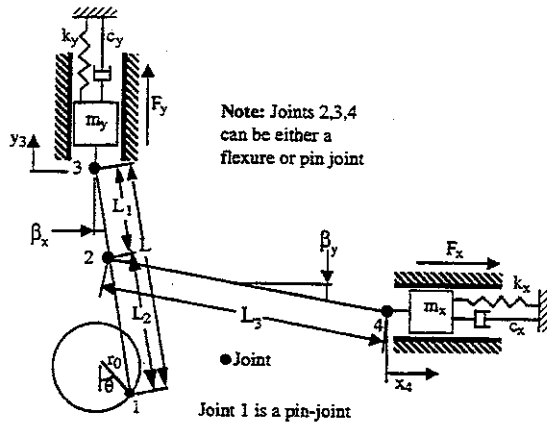
Figure 2. Flexure-Joint and Pin-Joint

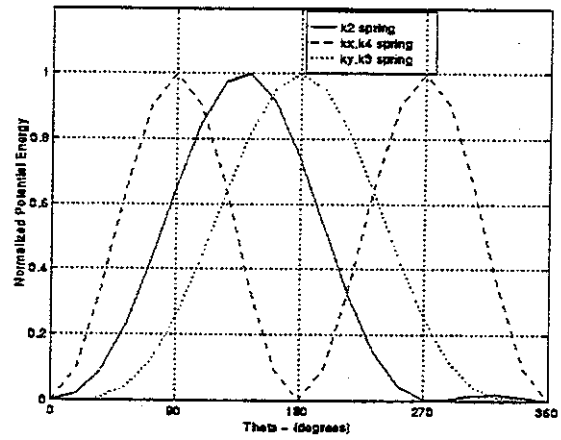Figure 3. Microengine Schematic

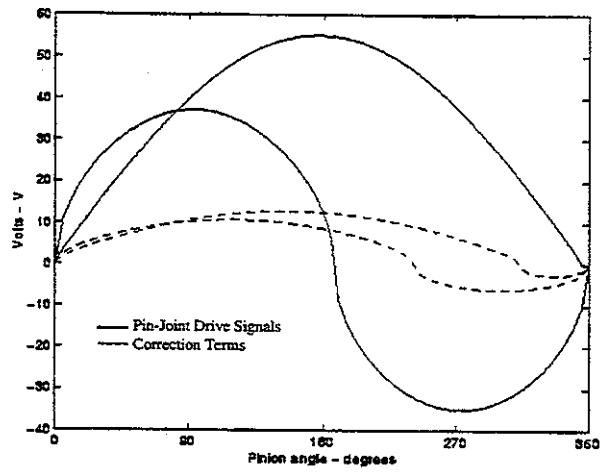Figure 4. Normalized Spring Potential Energy

Figure 5. Comparison of Pin-Joint and Flexure-Joint Drives Signals and the Measured Data
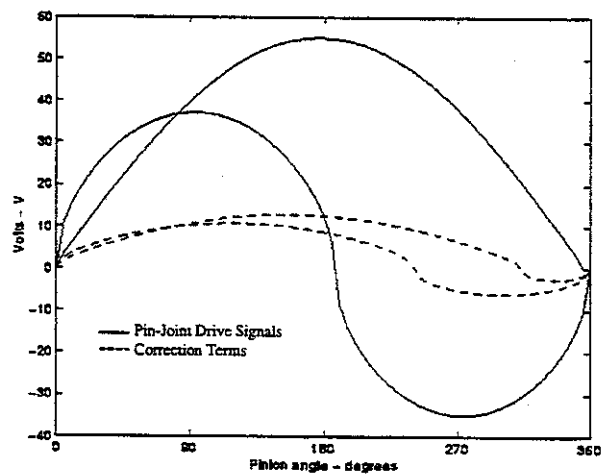

Figure 6. Pin-Jointed Drive Signals and the Correction Terms (λ_{1mod}/a, λ_{2mod}/a)